Aerospace Science and Technology 141 (2023) 108536

Contents lists available at ScienceDirect

Aerospace Science and Technology

journal homepage: www.elsevier.com/locate/aescte

An observation methodology for non-measurable rotorcraft states

Francesco Salucci [a], Paolo Parravicini [b], Carlo E.D. Riboldi [c], Lorenzo Trainelli [c]

[a] Argonne National Laboratory, 9700 S Cass Ave., Lemont, 60439, IL, USA
[b] Leonardo S.p.A., Aircraft Division, via Ingegnere Paolo Foresio 1, Venegono Superiore (VA), 21040, Italy
[c] Department of Aerospace Science and Technology, Politecnico di Milano, via La Masa 34, Milano (MI) 20156, Italy

ARTICLE INFO

Article history:
Received 2 March 2023
Received in revised form 21 July 2023
Accepted 21 July 2023
Available online 29 July 2023
Communicated by Antonio Filippone

Keywords:
Helicopter noise
Flap angles
Tip path plane
Thrust coefficient
Observer
Pilot acoustic indicator

ABSTRACT

In an attempt to reduce acoustic pollution due to terminal flight phases (lift-offs and landings) in the surroundings of heliport, project MANOEUVRES developed a device capable of estimating the acoustic footprint of helicopters on the ground. This device requires knowledge of certain quantities that cannot be directly measured through physical sensors: the tip-path plane angle of attack and the main rotor thrust coefficient. Previous research has demonstrated that these quantities can be accurately estimated using observers that are properly fed with directly measurable flight mechanics and rotor state variables. However, these observers, which are based on linear mathematical models identified offline and employed through interpolation with respect to nominal airspeed, have shown poor robustness when the number of identification input cases is reduced, as required for a realistic design of observers in the field. This issue has particularly emerged when non-trimmed manoeuvres were considered during observation testing. To address this issue, this paper introduces a new baseline for the observation model, which includes dynamic pressure as an additional input. Moreover, a different model structure is considered depending on the observed variable. Specifically, for the tip-path plane angle of attack, a single model covers the entire airspeed range, while observation models for the rotor thrust coefficient are interpolated based on flight altitude. This new approach demonstrates results of comparable or superior quality to previous observation models. Furthermore, it exhibits increased robustness when the pool of identification cases used for observer synthesis is significantly reduced. Such improved performance and ease of synthesis pave the way for the setup and adoption of the proposed observers in the field.

1. Introduction

Recent research efforts within the MANOEUVRES Clean Sky project [1] demonstrated that one method to reduce noise pollution on rotorcraft during critical manoeuvres, such as approach and landing, is the use of devices capable of providing the pilot with accurate information on the noise footprint of the helicopter during its operation. This would enable the pilot to execute a manoeuvre designed specifically to minimize the noise perceived on the ground.

These devices are conceived as composed of a new cockpit instrument, the Pilot Acoustic Indicator (PAI), that provides real-time acoustic impact information to the pilot, based on a noise estimation algorithm from the calculation of the current Sound Pressure Level (SPL) distribution around the aircraft.

The PAI has been conceived as secondary flight navigation instrument of practical use [2]. It provides the pilot with an estimated noise emission index and additional information on how to reduce it, suggesting vertical speed and direction adjustments. This may allow the pilot to react adequately in order to fly low-noise procedures, with limited impact on his/her workload. Given that the PAI is a secondary flight navigation instrument, it can be deactivated by the pilot depending on the situation and is fully integrated into the aircraft multi-function display. The PAI has been currently conceived as an instrument that simply gives a graphical indication to the pilot. A further development could be that of processing the noise emission index computed by the PAI through the Automatic Flight Control System (AFCS) and set up low-noise trajectories, thus reducing the pilot workload.

Key measurements for feeding the PAI include the angle of attack of the tip-path-plane (TPP-AOA), the main rotor thrust coefficient (C_T), as well as other aerodynamic properties such as true airspeed (TAS) and altitude [3,4].

E-mail address: carlo.riboldi@polimi.it (C.E.D. Riboldi).

https://doi.org/10.1016/j.ast.2023.108536

With the exception of airspeed and altitude, these variables cannot be measured directly. However, as shown in [4–6], it is possible to estimate these variables, adapting an approach introduced and validated in the field of rotors for wind power generation [7,8], and based on the knowledge of the flapwise motion of the main rotor blades, as well as possibly other aero-mechanical quantities.

In its formulation, this approach, initially applied in the field of rotorcraft in [5], is based on a linear observer, featuring a structure inspired by the equations for the dynamics of the flapping blade. These equations lead to a set of equivalences which can be employed to set up a linear system, where the unknown quantities to be observed are defined as functions of a set of measurable physical variables. In particular, working on a theoretical model of the flapping blade, it can be shown that the variables to be observed here, i.e. the TPP-AOA and the thrust coefficient, can be obtained from basic measurements of flight mechanics quantities and of the flapwise motion of the rotor, i.e. the rotor blade coning, longitudinal, and lateral flapping angles.

Despite the potential shown by the derived analytic model, it was found that more accurate results are obtained from observers synthesized employing model identification techniques, adopting observer structures as suggested by the theory (in particular, linear), but computing the coefficients from ad-hoc simulations performed in virtual environment. The model identification approach [9], often applied in the helicopter field to try increasing the fidelity of flight dynamics models with respect to purely theoretical predictions [10–12], carries a series of advantages that overcome some limits of a purely theoretical model. In particular, the theoretical model might employ assumptions and simplifications that do not match the complexity of the problem faced in the field. Furthermore, by employing a model identification approach, it is possible to configure the input of the observer and expand the set of measurement variables as required. This augmentation enables handling the sensitivity of the problem to unforeseen disturbances, such as sideslip angle and spurious accelerations, which may pollute the input to the observer in real field trials. This method may result in extremely accurate results, provided that the set of measurements fed to the observer (for model synthesis trials and when online) is carefully selected.

Developing this research thread further, the present paper has a threefold objective.

Firstly, it aims to retrace and explain the recent development in the formulation of the observer [5], carried out in an attempt to increase the accuracy of observations. This includes augmenting the array of measurements with the value of the tail rotor collective in [6]. In Section 2, this is briefly recalled and the corresponding observer model, named $K2$, is set as a benchmark to assess further improvements.

Secondly, this paper wants to show the effect of further extending the array of measurements with additional aero-mechanical parameters, namely main rotor collective angle, longitudinal cyclic angle, lateral cyclic angle, climb speed, climb angle, pitch angle, and roll angle. These variables have been added after an extensive trial and error phase, during which many combinations of the aforementioned variables have been tested. The resulting observer model, named $K14$, boosts the observation accuracy under both design and off-design conditions, despite a greater complexity due to the large number of measurements. This is explained in Section 3.

Thirdly, a new observer structure is proposed based on a further theoretical insight from the aerodynamic of the flapping blade, leading to a significant simplification of the model. In details, the dynamic pressure is added within the set of measurements fed to the model. This allows to linearly link the observed variables with a measurement that is representative of the helicopter airspeed. The corresponding new model, called $S15$, decouples the thrust coefficient estimation from that of the TPP-AOA, leading to two separate observation models. This research is presented in Section 4.

Finally, Section 5 compares the three just mentioned models on many quantitative results obtained in virtual environment using the numerical model of an existing rotorcraft testbed. The observer performance is initially evaluated on the same data samples used for the identification phase. Subsequently, it is tested on different data samples representing design conditions, and ultimately in off-design conditions where test manoeuvres very different from those considered in the identification phase are employed, introducing disturbances to constant-speed straight descents. Additionally, the model accuracy is assessed when using a reduced number of samples in the setup of the observer. This exploration aims to simulate a realistic synthesis procedure for the observer in the field, which may rely on a limited set of actual flight test data.

2. Theoretical structure of the observer and synthesis technique

In order to postulate the structure of an observer for a given set of desired aero-mechanical quantities, specifically the TPP-AOA α_{TPP} and thrust coefficient C_T, based on a set of assigned measurements, it is useful to study the underlying physical relationship between these variables.

To this aim, the equations for the flapping blade [13,14] provide a comprehensive view of the relationships between the variables defining the state of the helicopter from the viewpoint of flight mechanics and those characterising the flapwise motion of the blade. These equations can be conveniently grouped in the system of equations

$$\boldsymbol{Q}\,\boldsymbol{s} = \tilde{\boldsymbol{T}}\tilde{\boldsymbol{m}} + \tilde{\boldsymbol{q}}. \tag{1}$$

The array $\boldsymbol{s}^T = \{\alpha_{TPP}, C_T\}$ includes the quantities to be observed and array $\tilde{\boldsymbol{m}}^T = \{a_0, a_{1_s}, b_{1_s}, \theta_0, B_1\}$ is made of the measurements necessary for the observation. These measurements include the rotor blade coning angle a_0, the longitudinal flap angle a_{1_s}, the lateral flag angle b_{1_s}, the collective pitch angle θ_0, and the longitudinal cyclic angle B_1. The coefficients of the matrices $\boldsymbol{Q}$ and $\tilde{\boldsymbol{T}}$ and of the array $\tilde{\boldsymbol{q}}$ can be expanded as

$$\boldsymbol{Q} = \begin{bmatrix} \frac{\mu^2}{2} & -\frac{1}{4} \\ 0 & 1 \end{bmatrix}$$

$$\tilde{\boldsymbol{T}} = \begin{bmatrix} 0 & (\frac{3}{8}\mu^2 + \frac{1}{4}) & -(\frac{2eM_b}{g\gamma I_b(1-\frac{e}{R})^2}) & -\frac{2}{3}\mu & (\frac{7}{8}\mu^2 + \frac{1}{4}) \\ \frac{\sigma(I_b + e\frac{M_b}{g})}{\frac{2}{3}\rho c R^4(1-\frac{e}{R})} & 0 & 0 & 0 & 0 \end{bmatrix}$$

$$\tilde{\boldsymbol{q}} = \begin{Bmatrix} -\frac{1}{2}\mu\theta_1 \\ -\frac{\sigma\frac{M_b}{\Omega^2}}{\frac{2}{3}\rho c R^4(1-\frac{e}{R})} \end{Bmatrix} \tag{2}$$

where $\mu = \frac{V}{\Omega R}$ is the advance ratio, comparing the TAS of the translational motion of the helicopter V with the tip speed of the blade, given by the product of the rotor radius R and the rotor rotational speed Ω. In the same matrix $\tilde{\boldsymbol{T}}$, the term e is the dimensional hinge offset, while M_b and I_b are the static moment of inertia and the moment of inertia for the flapping section of the blade respectively. The parameter $\sigma = \frac{cN_b}{\pi R}$ is the solidity of the rotor, where c is the chord of the blade and N_B is the number of blades. The term $\gamma = \frac{\rho a c R^4}{I_b}$ is the Lock number, the ratio between aerodynamic forces acting to lift up the rotor blades and inertial forces. Finally, vector $\tilde{\boldsymbol{q}}$ contains also the blade linear twist angle θ_1.

Full derivation of Equation (2) can be found in [5]. The validity of Equation (2) is limited by the following assumptions:

- advanced, steady flight;
- linear aerodynamics (no stall and compressibility effects);
- absence of a reverse flow region on the rotor;
- blade motion consists only of first harmonic flapping and coning;
- small-angle assumption.

By considering steady flight, Equation (2) does not include the effect of pitch and roll velocities on flapping angles. This effect was neglected for the sake of simplicity, considering the standard approach manoeuvres analysed in this work.

From the definition of matrix $\boldsymbol{Q}$ it is clear that no singularity can be expected unless $\mu = 0$, which happens only for hover conditions. As a consequence, it is always possible to left-multiply Equation (1) by the inverse of $\boldsymbol{Q}$, yielding

$$\boldsymbol{s} = \boldsymbol{T}\tilde{\boldsymbol{m}} + \boldsymbol{q} \tag{3}$$

where $\boldsymbol{T} = \boldsymbol{Q}^{-1}\tilde{\boldsymbol{T}}$ and $\boldsymbol{q} = \boldsymbol{Q}^{-1}\tilde{\boldsymbol{q}}$.

The system can be rewritten in homogeneous form, by augmenting the array of measurements $\tilde{\boldsymbol{m}}$ with a unitary element and grouping the matrix $\boldsymbol{T}$ with the vector $\boldsymbol{q}$, hence

$$\boldsymbol{s} = \boldsymbol{K}\boldsymbol{m} \tag{4}$$

where

$$\boldsymbol{K} = [\boldsymbol{T}|\boldsymbol{q}] \tag{5}$$

and

$$\boldsymbol{m} = \begin{Bmatrix} \tilde{\boldsymbol{m}} \\ 1 \end{Bmatrix}. \tag{6}$$

Equation (4) clearly indicates a suitable structure for the proposed observer. Based on the considered derivation from the flapping blade equation, the coefficients of the model matrix $\boldsymbol{K}$ depend largely on constant geometrical and inertial properties of the considered helicopter rotor, namely I_b, M_b, σ, e, c and R. Furthermore, they are functions of airspeed – through the advance ratio μ – and altitude – both explicitly through ρ and through the Lock number γ. Finally, assuming that the inertial properties stay constant during the approach manoeuvres of interest, Equation (4) becomes

$$\boldsymbol{s} = \boldsymbol{K}(\mu, \rho)\boldsymbol{m}, \tag{7}$$

highlighting the baseline observer structure suggested by theory.

2.1. Synthesis of the observation model: approach through parameter identification

The proposed analytic description of the observer structure represented by Equation (4) and the corresponding coefficients of matrix $\boldsymbol{K}$ offers some insight into the potential measurements necessary to feed the observer. However, this analytic formulation is too simplistic to be safely adopted in real practice. Indeed, the analysis outlined above is obtained taking into account only the isolated rotor and incorporates various simplifications and assumptions made during the development of the analytic model for the flapping blade [14].

To cope with this, an approach based on model identification has been devised to determine the coefficients of matrix $\boldsymbol{K}$, by utilizing realistic datasets. One noteworthy characteristic of the model identification approach is that the coefficients of matrix $\boldsymbol{K}$ are computed based on the selection of data used to train the observer. This dataset, referred to as the identification dataset, has to cover a wide range of α_{TPP} and C_T values, possibly considering a sufficient number of different flight conditions, capturing the essence of the relationship between the measurements $\boldsymbol{m}_i$ and the observed variables $\boldsymbol{s}_i$.

Then, through a suitable identification method, it is possible to compute the model matrix of a linear model $\boldsymbol{K}(\bar{\mu}, \bar{\rho})$ for a given value of the airspeed and altitude.

If the identification algorithm is suitable for the problem at hand, the model identification approach proves valuable in identifying and accounting for dependencies that may not have been explicitly captured in a purely analytic model.

Collecting the values of $\boldsymbol{s}_i^T = \{\alpha_{TPP_i}, C_{T_i}\}$ and $\boldsymbol{m}_i^T = \{\tilde{\boldsymbol{m}}, 1\}$ for $i = 1, \cdots, N_p$, where N_p is the number of considered samples for the assigned advance ratio $\bar{\mu}$ and air density $\bar{\rho}$, the model matrix $\boldsymbol{K}(\bar{\mu}, \bar{\rho})$ will be such that

$$\left[\boldsymbol{s}_1 \cdots \boldsymbol{s}_{N_p}\right] = \boldsymbol{K}(\bar{\mu}, \bar{\rho})\left[\boldsymbol{m}_1 \cdots \boldsymbol{m}_{N_p}\right]. \tag{8}$$

This can be rewritten synthetically as

$$\boldsymbol{S} = \boldsymbol{K}(\bar{\mu}, \bar{\rho})\boldsymbol{M}, \tag{9}$$

and the values of the coefficients of the model matrix for the assigned $\bar{\mu}, \bar{\rho}$ can be obtained through a suitable identification method. For the problem under analysis a least-squares method has been considered. This yields

$$\hat{\boldsymbol{K}}(\bar{\mu}, \bar{\rho}) = \boldsymbol{S}\boldsymbol{M}^T(\boldsymbol{M}\boldsymbol{M}^T)^{-1} \tag{10}$$

where the $\hat{(\cdot)}$ sign indicates that the coefficients have been estimated.

Once the coefficients of the model matrix are known, matrix $\hat{\boldsymbol{K}}(\bar{\mu}, \bar{\rho})$ can be employed online to obtain an estimation of the desired quantities $\hat{\boldsymbol{s}}$ from a measurement of the parameters $\boldsymbol{m}$

$$\hat{\boldsymbol{s}} = \hat{\boldsymbol{K}}(\bar{\mu}, \bar{\rho})\boldsymbol{m}, \tag{11}$$

in the same fashion as highlighted by Equation (7).

2.2. Airspeed parameterization

As outlined in Section 2.1, the coefficients of the matrix $\boldsymbol{K}$ contain altitude and airspeed terms. In particular, both matrix $\boldsymbol{T}$ and the array $\boldsymbol{q}$ in Equation (3) depend nonlinearly on μ and ρ. As a consequence, each observation model is valid just for a particular airspeed and altitude.

Both airspeed and altitude may vary during the approach manoeuvres of interest here. Previous studies on the subject [5], suggest that even significantly different altitude values produce a small change on the coefficients of the model matrices, whereas the effect of airspeed is much more pronounced. Following this assumption, the dependence of the model coefficients from altitude can be neglected, yielding the expression $\boldsymbol{T} = \boldsymbol{T}(\mu)$ and $\boldsymbol{q} = \boldsymbol{q}(\mu)$. Referring to the homogeneous form of the observer within Equation (4), the dependence with respect to μ will bear $\boldsymbol{K} = \boldsymbol{K}(\mu)$.

To effectively handle the varying parameter values, particularly airspeed, during model identification runs, a decision was made to organize the samples comprising the time histories of the measured signals into predetermined speed buckets. This approach aimed to appropriately distribute the data based on their corresponding airspeed values.

Such buckets are centred in N_v equally spaced speed nodes, each corresponding to an assigned speed of the stream $\bar{V} = V_v$. Depending on the instantaneous airspeed, every measurement sample $\boldsymbol{s}_i$ falls in the corresponding speed bucket, such that $V \in$

Table 1
Comparison in the composition of the arrays of measurements $\boldsymbol{m}$ for the $K2$ and $K14$ models.

Model	a_0	a_{1s}	b_{1s}	ρ	W	θ_{TR}	θ_0	$B1$	$A1$	V_z	γ_{fus}	θ_{fus}	ϕ_{fus}
K2	X	X	X	X	X	X							
K14	X	X	X	X	X	X	X	X	X	X	X	X	X

$\left[\bar{V} - \Delta V, \bar{V} + \Delta V\right]$. Buckets do not overlap and have an amplitude $\Delta V = \frac{1}{2}(V_{v+1} - V_{v-1})$.

All samples attributed to a certain airspeed bucket will contribute to the identification of the model corresponding to the reference airspeed $\bar{V} = V_v$ and the corresponding $\bar{\mu}_v$, according to Equation (8).

To make use of the observer in an operational scenario where the advance ratio μ undergoes changes, it is necessary to store the coefficient values of $\boldsymbol{K}$ for a number of $\bar{\mu}_v$ buckets. The number of buckets should encompass the helicopter operational speed range for the considered class of manoeuvres (e.g. approach and landing). During runtime, the model matrix associated with the actual value of the advance ratio μ will be interpolated online. In [5,6] a linear interpolation was considered between identification nodes, yielding

$$\boldsymbol{K}(\mu) = \boldsymbol{K}_v + (\boldsymbol{K}_{v+1} - \boldsymbol{K}_v)\frac{\mu - \bar{\mu}_v}{\bar{\mu}_{v+1} - \bar{\mu}_v}, \ \bar{\mu}_v \leq \mu < \bar{\mu}_{v+1} \quad (12)$$

for the model matrix related to the actual value of μ.

3. Augmenting the set of measurements

As highlighted in Section 2.1, it is possible to improve the results by modifying the array of measurements $\boldsymbol{m}$ beyond what is suggested by theory. For instance, as shown in [5], additional measurement variables may be included to address sensitivity to exogenous parameters. This modification can be implemented while keeping the identification procedure presented in Equation (8), (9) and (10) unchanged.

Thanks to the technology developed in previous research projects [4], we can consider the flap angles as available measurements. Moreover, since all our manoeuvres of interest (see Section 5.1) can be assumed to be quasi-static, no significant dynamic phenomena should appear in the flapwise motion of blades. Hence, it can be safely assumed that the helicopter is moving in a trimmed flight condition. This in turn allows to hypothesize that there exists a relationship between the coefficients of the trimmed pitch input and those of the flapwise deflection. At first, this remark yields a reduction of the array of measurements $\boldsymbol{m}$ in Equation (6) to

$$\boldsymbol{m} = \left\{a_0, \quad a_{1_s}, \quad b_{1_s}, \quad 1\right\}^T. \quad (13)$$

However, from empirical studies [5], it turns out that flap angles show a marked dependency also on the helicopter mass and altitude. Hence, to improve the model quality and to account for these dependencies on altitude and weight, air density ρ and weight W were added to the array of measurements yielding the new vector

$$\boldsymbol{m} = \left\{a_0, \quad a_{1_s}, \quad b_{1_s}, \quad W, \quad \rho, \quad 1\right\}^T. \quad (14)$$

By inspecting the quality of the measured signals in $\boldsymbol{m}$ from simulations in [6], it was noted that better knowledge of the lateral-directional state of the helicopter would be beneficial for the accuracy of the estimation. A way to provide such information starting from quantities typically available from the avionic data bus of a helicopter – thus without making the sensor chain more complicated – has been found in the augmentation of m with the tail rotor collective θ_{TR}. The simplest way to add this quantity to the array of measurements, similarly to what had been done already for the quantities ρ and W, is that of supposing a linear behaviour of the observation model with respect to it, yielding

$$\boldsymbol{m} = \left\{a_0, \quad a_{1_s}, \quad b_{1_s}, \quad W, \quad \rho, \quad \theta_{TR}, \quad 1\right\}^T. \quad (15)$$

Results from this scenario show remarkably limited errors in both design and off-design conditions. For instance, in design conditions, the relative error on C_T is always less than 0.2% and that on α_{TPP} always less than 5% [6].

More recently, with the goal to improve the general quality of the observer even more, further attempts have been carried out to identify the optimal set of measurements, including helicopter attitude angles, trajectory angles, and controls. These additional measurements include:

- blade root collective pitch θ_0
- blade longitudinal cyclic pitch B_1
- blade lateral cyclic pitch A_1
- helicopter vertical speed V_z
- helicopter descent angle γ_f
- helicopter pitch angle θ_f
- helicopter roll angle ϕ_f

Starting from this rich set, an extensive comparative analysis of many different observer models using different combinations of measurements has been performed. A total of 14 models have been derived, differing by the considered set of measurements. Each model has been designed as linearly scheduled with respect to the airspeed as explained in Section 2.2.

For the sake of brevity, this paper compares only two especially interesting models named as $K2$ and $K14$. In particular, the $K2$ model uses the array of measurements in Equation (15), for a total of 6 measurements. The $K14$ model adds other 7 measurements for a total of 13. The corresponding sets of measurements employed are detailed in Table 1. Results on the effect of the augmentation will be presented in Section 5, assessing also the robustness of the observation chain through simulations in off-design conditions.

It is worth noting that the observer relies on the availability of on-board measurements of the rotor flapping motion, pilot commands, air density, weight, and other quantities such as TAS, rate of climb, pitch angle, and roll angle. The estimation of these parameters is usually not straightforward, as they might not be directly measurable themselves. Many of these quantities need to be derived from the aircraft air data system, fuel system, navigation system, and – in the case of flap angles – from the recently developed rotor state measurement system described in [4], which is still in early development stage. Uncertainties in each of the measurements should be quantified by defining error bounds and/or confidence intervals. This unreliability of the measurements can propagate through the observer algorithm and affect the estimated values of α_{TPP} and C_T. In this work, we will assume that each measured variable is known without bias. Nevertheless, we believe that a thorough assessment of the observer accuracy should be done by considering the complete chain of uncertainties, especially in light of a possible real-life application.

4. Additional amendments to model structure

Before showing some results, further considerations on the structure of the model will be reported here. This further investigation has been suggested by the results obtained in practice, when trying to obtain more accurate observation at a lower computational cost. In this regard, it should be recalled that the observer synthesis may require a high number of dedicated runs (either in a high fidelity simulation environment or in the field). An increased number of parameters in the measurements $\boldsymbol{m}$ implies a higher number of coefficients to be identified in $\boldsymbol{K}$, and this in turn increases the number and diversity of cases to be fed to the identification procedure. The airspeed-scheduled structure of the observer outlined in the previous sections is another source of complexity which, as will be briefly outlined here, can be revisited to better cope with the physics of the observation model at hand.

The following paragraphs explain the pathways followed in the rationalization of the model structure.

4.1. Dynamic pressure as an input

As it is going to be shown in Section 5, the effect of simply adding new measured variables to the set of measurements $\boldsymbol{m}$, appears to bring limited benefit to the quality of the observation.

A reason for this is the nonlinear dependency of the model matrix $\boldsymbol{K}$ coefficients on the advance ratio μ, and ultimately on the airspeed V.

In the models described above, the information about airspeed is embedded in the model matrix $\boldsymbol{K}$ and there exists a different matrix $\boldsymbol{K}$ for each value of the airspeed, considered by building different buckets with respect to a nominal value of the advance ratio $\bar{\mu}$, as shown.

However, the linear interpolation of matrix $\boldsymbol{K}$ as described in Equation (12), is not perfectly suited to deal with this nonlinearity. Given the linear nature of the selected identification method, we sought a way to retrieve linearity with respect to airspeed. Again, a useful insight in this sense comes from the physics behind the flapping blade equations used to set up the observer structure. In particular, as known, the lift acting on the i-th blade L_i, is proportional to the dynamic pressure q_{dyn} as

$$L_i = q_{dyn} A_b \bar{C}_L \tag{16}$$

where A_b is the surface of the blade and $\bar{C}_L$ the average lift coefficient. The dynamic pressure is, by definition, a quadratic function of the airspeed V as

$$q_{dyn} = \frac{1}{2}\rho V^2. \tag{17}$$

The linear relationship between lift and dynamic pressure suggests the choice of q_d as an additional element of the vector $\boldsymbol{m}$.

Since the information about airspeed V is now embedded into the q_{dyn} measurement, the model parameterization with respect to airspeed V as described in Section 2.2 is no longer required. This means that a unique matrix $\boldsymbol{K}$ can be identified, for all the airspeed conditions considered for identification, without resorting to the airspeed buckets employed in Equation (12).

4.2. Altitude parameterization

Section 2 pointed out that the matrix $\tilde{\boldsymbol{T}}$, and ultimately the model matrix $\boldsymbol{K}$ is a function of both the airspeed, through the advance ratio μ, and altitude, through the density of air ρ.

In particular, the first row of matrix $\tilde{\boldsymbol{T}}$, includes the effect of air density through the Lock number γ. The second row of the matrix, pertaining to the thrust coefficient C_T, shows the altitude term ρ, always at the denominator. This comes as a consequence of the definition of the thrust coefficient as

$$C_T = \frac{T}{\pi R^2 \rho (\Omega R)^2} \tag{18}$$

where T is the main rotor thrust. Equation (18) highlights another nonlinear relation between ρ (i.e. altitude) and C_T.

Once again, empirical studies described in Section 5 will show that, for what concerns the estimation of C_T, it is possible to repeat the bucketing technique of Equation (12) using altitude z as an independent variable for interpolation. Similar to the airspeed buckets, the altitude buckets are centred in N_z equally spaced altitude levels, each corresponding to an assigned altitude $\bar{z} = z_z$.

Depending on the instantaneous altitude, every measurement $\boldsymbol{s}_i$ falls in the corresponding altitude bucket such that $z \in [\bar{z} - \Delta z, \bar{z} + \Delta z]$.

All samples attributed to a certain altitude bucket will contribute to the identification of the model corresponding to the reference altitude $\bar{z} = z_z$.

Also in this case, a linear interpolation was considered between altitude levels, yielding

$$\boldsymbol{K}(z) = \boldsymbol{K}_z + (\boldsymbol{K}_{z+1} - \boldsymbol{K}_z)\frac{z - \bar{z}_z}{\bar{z}_{z+1} - \bar{z}_z},\ \bar{z}_z \le z < \bar{z}_{z+1} \tag{19}$$

for the model matrix related to the actual value of z.

4.3. Split model: different measurements for each observed variable

Following the reasoning regarding the use of dynamic pressure as additional measurement and the non-linearity of the C_T with respect to altitude, it was decided to separate the models for the observation of α_{TPP} and C_T.

Following several simulations and tests of the observer in design and off-design conditions, the observer model has been split according to the observed variable as follows

- α_{TPP}: dynamic pressure q_{dyn} is added to the vector of measured variables $\boldsymbol{m}$ and there is no parameterization with respect to airspeed or altitude, i.e. there is a single matrix $\boldsymbol{K}$ identified using all the data at different airspeed and altitude;
- C_T: dynamic pressure q_{dyn} is added to the vector of measured variables $\boldsymbol{m}$ but the identification data is divided into buckets according to altitude. For every altitude bucket a model matrix $\boldsymbol{K}$ is identified. The observer employs the linear interpolation of Equation (19) in each observation case. Air density ρ is therefore eliminated from the vector of measurements, since its contribution is already steering the model parameterization.

The so-obtained split model, making use of two different observer structures for the TPP-AOA and the thrust coefficient, has been named $S15$. This identification wraps the two separate models just introduced for the observation of α_{TPP} and C_T, which are based on different sets of measurements, i.e. a different content of array $\boldsymbol{m}$.

5. Results

5.1. Flight conditions for model identification

Since the goal of the PAI recalled in Section 1 is that of reducing helicopter noise during final approaches, the reference flying condition is that of a continuous trimmed descent, as depicted in Fig. 1.

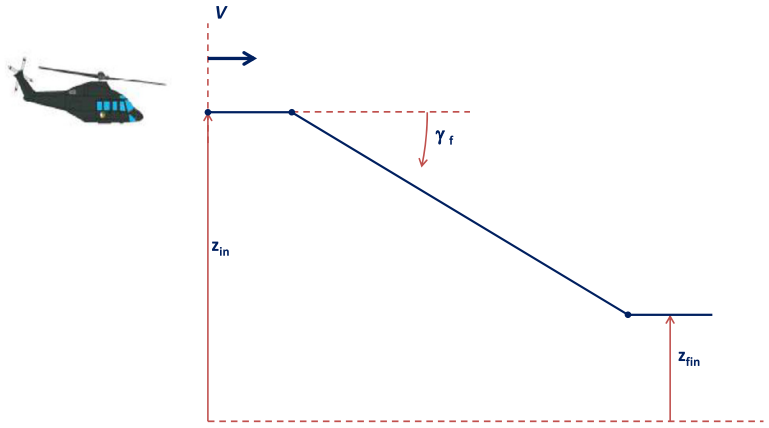

Fig. 1. Trimmed descent profile considered for identification.

Table 2
Flight parameters considered for the identification phase.

V [kn]	β_f [°]	W [kg]	z [ft]	γ_f [°]
30	-10	2,183	3,000	3
40	0	2,282	2,500	4
50	10	2,381	2,000	5
60		2,481	1,500	6
70		2,580	1,000	7
80		2,679	500	
90		2,778		
100		2,877		
110		2,977		
120		3,076		
		3,175		

Similarly to [6], the observer has been developed and tested in virtual environment using the simulator `RSim` [15]. `RSim` implements a rigid model suitable for analysing the flight dynamics of the helicopter, plus a model of the flexible main rotor based on the theory found in [14,13] to simulate the rotor flapping dynamics.

The validated model of an existing lightweight, twin-engine, multi-purpose helicopter has been considered for all tests.

Each manoeuvre is simulated through a series of trimmed descent points, starting at an altitude $z_{in} = 3{,}000$ ft with a 500 ft decrement. The values of the helicopter TAS vary between 30 and 120 kn. The helicopter is assumed to descend in steady flight. Since the descent angle γ_f has a straightforward relationship with α_{TPP} — a larger descent angle should involve a larger angle of attack and therefore a bigger α_{TPP} — angles from 3° to 7° were considered. Each descent was simulated at different angles of sideslip, varying from -10° to +10° every 10°. All the parameter values assumed for the simulated flight conditions for identification (i.e. for observer synthesis) are collected in Table 2.

With the whole set of combinations, a total of 9900 trim conditions have been simulated.

5.2. Observation models

The observation models $K2$, $K14$ and $S15$ outlined in Sections 3 and 4.1 are here compared in their capacity to replicate the observed quantities α_{TPP} and C_T. For an easier referencing, Table 3 tries to summarise the differences between the three models.

As shown in Section 2.2, identification data is organised in airspeed buckets for what concerns model $K2$ and $K14$. Each bucket corresponds to a nominal value of the TAS and contains all the data points with a TAS close to the nominal value within a maximum tolerance $\Delta V = 10$ kn.

On the other hand, model $S15$ makes use of altitude buckets (see Section 4.2) for the observation of the thrust coefficient C_T. In this case, each bucket is $\Delta z = 500$ ft in width.

5.3. Quality of the identified model

Before proceeding to the evaluation of the observation results, the observer operation is checked on the same samples considered for identification. This observation should produce very accurate results except in case of issues to the selected structure of the observer, adopted identification technique, or unsuitability of the pool of cases considered for identification.

For every airspeed bucket (model $K2$ and $K14$), and altitude bucket (model $S15$ - C_T only) a matrix $\boldsymbol{K}$ was identified using the aforementioned least-squares technique. These matrices are now tested on the same samples used to compute them.

The $K2$, $K14$, and $S15$ models are tested on all airspeed buckets. Results are shown in Fig. 2. Because of the large number of simulations, $K2$ and $K14$ results are displayed for the 30 kn airspeed bucket only. Conversely, for $S15$ model, the whole set of identification data is reported in a single plot.

In Fig. 2, the horizontal and the vertical axes represent the real and the observed values of the considered variable respectively, in this case α_{TPP}. The red line is the ideal correlation line, while the blue squares are the observed samples. The closest the squares are to the correlation line, the more accurate the quality of the observation is.

The analysis of Fig. 2 indicates that $K2$ model features the lowest degree of accuracy, compared to $K14$ and $S15$, with more data points lying further away from the ideal correlation line. On the contrary, the samples are much more concentrated around the ideal correlation line in Fig. 2(b) and (c). The disparity between $K2$ and the other two models may be due to the smaller number of input measurements that the $K2$ model employs (6 variables), compared to $K14$ and $S15$ (13 and 14 respectively).

Interestingly, the $K14$ model appears more accurate than the $S15$ model, despite the presence of one additional measurement, namely the dynamic pressure. However, it can be observed that in Fig. 2 a single $S15$ model matrix is identified based on the entire set of flight conditions, covering different values of the airspeed, ranging across all speed buckets. On the other hand, multiple $K14$ model matrices are identified for every speed bucket, and here the $K14$ model is being tested on the same data points used for identification, in this case the 30 kn cases.

In order to further assess the quality of the observer performance, the value of the absolute error for every airspeed bucket has been calculated, as shown in Fig. 3. In particular, Fig. 3(a) shows the error on α_{TPP} while Fig. 3(b) shows the error on C_T.

Table 3
Summary of the proposed observer models.

Model ID	Observed variables	Measured variables	Bucketing parameter
K2	α_{TPP}. C_T	$\{a_0, a_{1s}, b_{1s}, \rho, W, \theta_{TR}\}$	Airspeed V
K14	α_{TPP} C_T	$\{a_0, a_{1s}, b_{1s}, \rho, W, \theta_{TR}, \theta_0, B_1, A_1, V_z, \gamma_f, \theta_f, \phi_f\}$	Airspeed V
S15	α_{TPP} C_T	$\{a_0, a_{1s}, b_{1s}, \rho, W, \theta_{TR}, \theta_0, B_1, A_1, V_z, \gamma_f, \theta_f, \phi_f, q_{dyn}\}$ $\{a_0, a_{1s}, b_{1s}, W, \theta_{TR}, \theta_0, B_1, A_1, V_z, \gamma_f, \theta_f, \phi_f, q_{dyn}\}$	None Altitude z

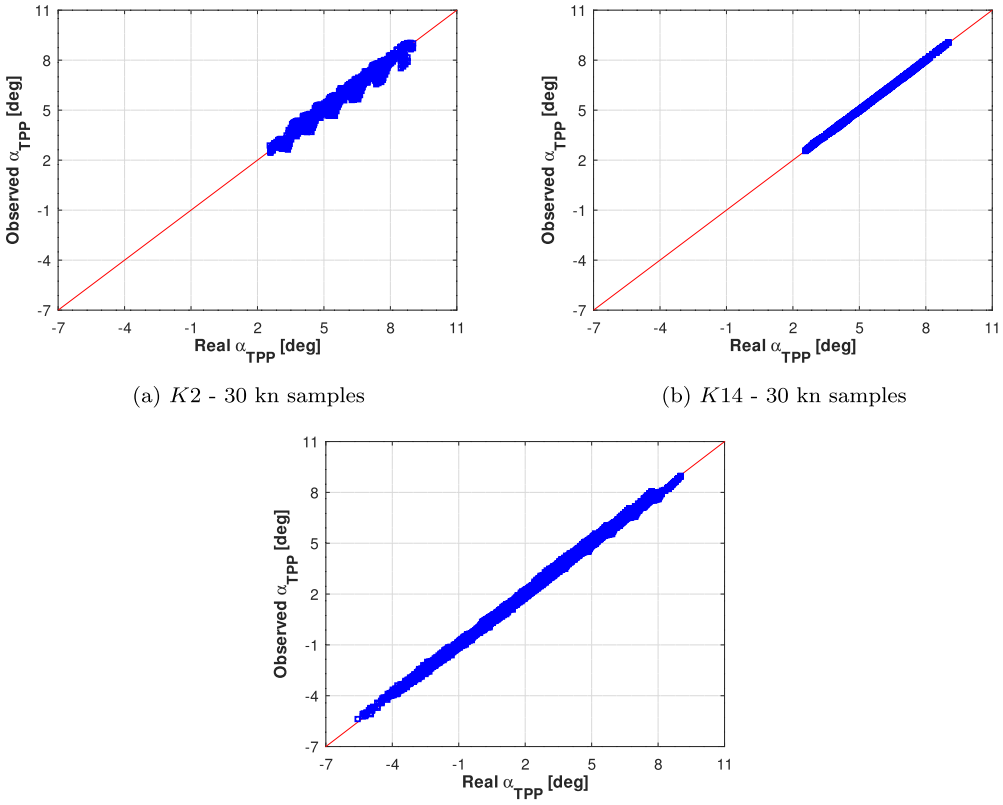

(a) $K2$ - 30 kn samples

(b) $K14$ - 30 kn samples

(c) $S15$ - all samples

Fig. 2. Model quality check for α_{TPP} on identification data. (For interpretation of the colours in the figure(s), the reader is referred to the web version of this article.)

The black bars refer to the $K2$ observer, the blue bars to $K14$ and the yellow bars to $S15$. Firstly, the graphs highlight that the error values are remarkably limited, in all cases. Nevertheless, the higher value of the error with $K2$ model is apparent in the low-speed buckets for α_{TPP} and all the speed buckets for C_T, showing that the small number of measured variables may reduce accuracy in observation. $K14$ features the best values of the absolute error on α_{TPP}, but it is outperformed by $S15$ when considering C_T. Fig. 3(c) and (d) show that the magnitude of the relative error on the two parameters can be used to drive the same conclusions. Considering the small numerical values assumed by $\alpha_{TPP} \approx [1, 10]$ deg and $C_T \approx [0.004, 0.009]$, we will only display absolute error graphs for the remainder of the paper.

The error values in Fig. 3 confirm what emerged from the qualitative analysis of Fig. 2. $K14$ appears to be a better model for the α_{TPP} estimation with respect to $S15$. However, it must be considered that the dataset used for $K14$ identification uses a smaller but more homogeneous number of samples, with all the points falling within the same speed bucket. Therefore, $K14$ model is expectedly very precise in reproducing the same data employed for identification. On the other hand, model $S15$ is identified with a wider set of data containing the whole range of airspeeds. Thus, the data provided to the model covers a wider set of conditions. This brings to a lower observation accuracy when tested on the same identification data, but should comparatively increase model generality and adaptability in different flight conditions, as will be shown shortly.

5.4. Observation in design conditions

To assess the quality of the observation algorithm, more simulations have been performed at intermediate airspeeds and intermediate angles of sideslip, not considered for identification. Even though they were carried out at intermediate airspeeds and sideslip angles, these conditions nonetheless consist of trimmed descent flights. They are therefore referred to as design conditions (as opposed to off-design conditions, shown later).

The airspeed values and sideslip angles considered for these additional simulations are collected in Table 4(a) and (b).

Simulations are conducted for all the weights, altitudes and descent angles considered during the identification phase and reported in Table 2.

A total of 7920 simulations are carried out for this testing phase.

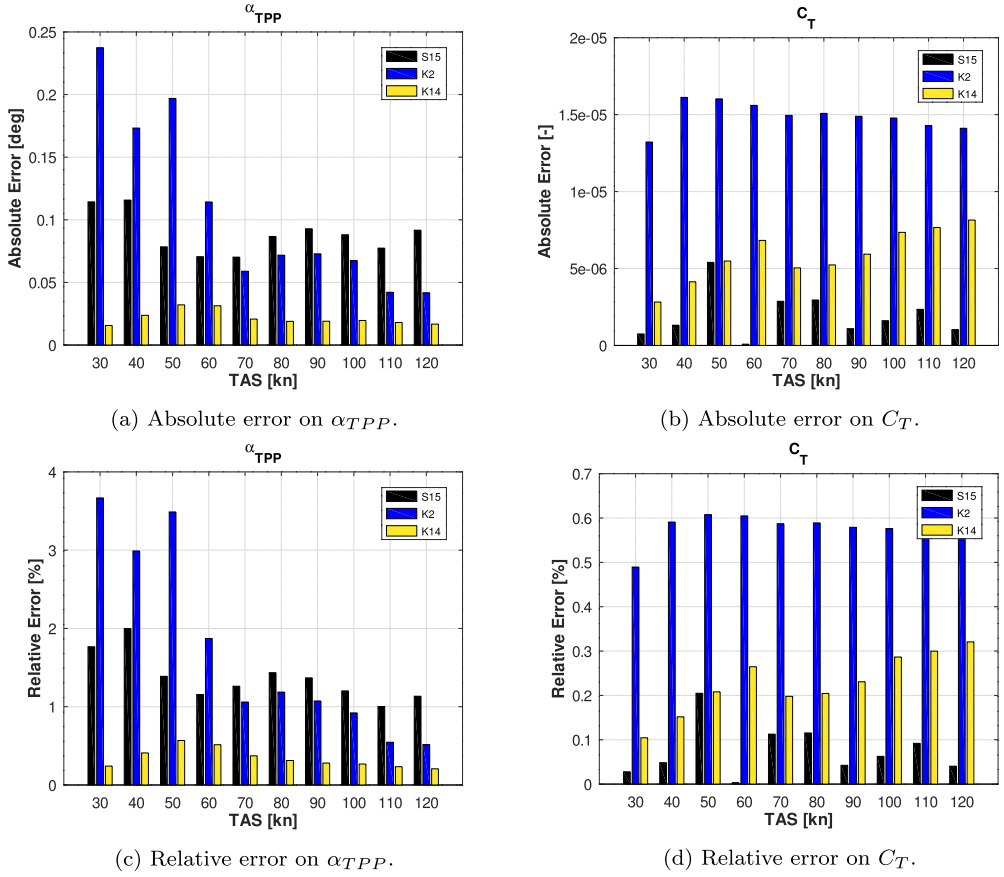

(a) Absolute error on α_{TPP}.

(b) Absolute error on C_T.

(c) Relative error on α_{TPP}.

(d) Relative error on C_T.

Fig. 3. Average absolute and relative error for simulations at various airspeeds. Observer checked on the same samples considered for identification.

Table 4
Flight parameters considered for observation in design conditions.

(a) Intermediate airspeed cases.

V [kn]	β_f [°]
35	0
45	
55	
65	

(b) Intermediate sideslip angle cases.

V [kn]	β_f [°]
30	-5
40	5
50	
60	
70	
80	
90	
100	
110	
120	

5.4.1. Intermediate airspeed conditions

The intermediate airspeed cases, at 35, 45, 55 and 65 kn, with $\beta = 0°$ are important to study the dependency of the model matrix $\boldsymbol{K}$ with respect to the advance ratio μ or, ultimately, the airspeed V.

The model coefficients of $K2$ and $K14$ have been linearly interpolated as explained in Equation (12), based on the actual value of the airspeed of each sample in the new simulations.

Results in Fig. 4 show the agreement between real and observed values for the $K2$, $K14$, and $S15$ models at intermediate airspeeds (blue squares at 35 kn, black diamonds at 45 kn, light blue circles at 55 kn and green triangles at 65 kn). It emerges that model $K2$ samples are less concentrated around the identity line than $K14$ and $S15$ samples, especially for low-speed conditions (35 kn). Contrarily, model $K14$ and $S15$ show a better level of accuracy with respect to $K2$, although the $K14$ observed samples for the low-speed cases (35 kn) lie below the identity line, highlighting an underestimation of α_{TPP} that appears proportionate to the magnitude of the quantity itself;

This fact is particularly evident if we look at relative errors in Fig. 5. Looking at the black bars representing the $S15$ model, the absolute error on α_{TPP} observation is always lower than the $K2$ or $K14$ errors, except for the 65 kn case, where the three models perform equally well.

Concerning the C_T observation, shown in Fig. 5(b), model $S15$ clearly outperforms the other two.

5.4.2. Intermediate angle of sideslip conditions

Further simulations have been run in two scenarios different from that considered for identification. In particular, simulations with $\beta =$ -5°, +5°. These are still considered design conditions, since samples with $\beta = \pm 10°$ were included in the identification process.

Fig. 6(a) shows the comparison between the absolute error of $K2$, $K14$ and $S15$ models for α_{TPP}. As it can be observed therein, the additional measurements used by the $K14$ model contribute to cut the value of the absolute error, especially compared to the $K2$ model. This occurs for all the airspeed buckets. On the other hand, the absolute error of $S15$ is less than that of $K2$ between 30 kn and 60 kn and over 100 kn.

Conversely, in Fig. 6(b) the absolute error on the C_T observation for the $S15$ model plunges below $K2$ and $K14$ in all cases.

5.5. Observation in off-design conditions

In order to test the observer robustness, a few simulations that bring the helicopter out of design conditions have been considered. Two off-design scenarios have been developed:

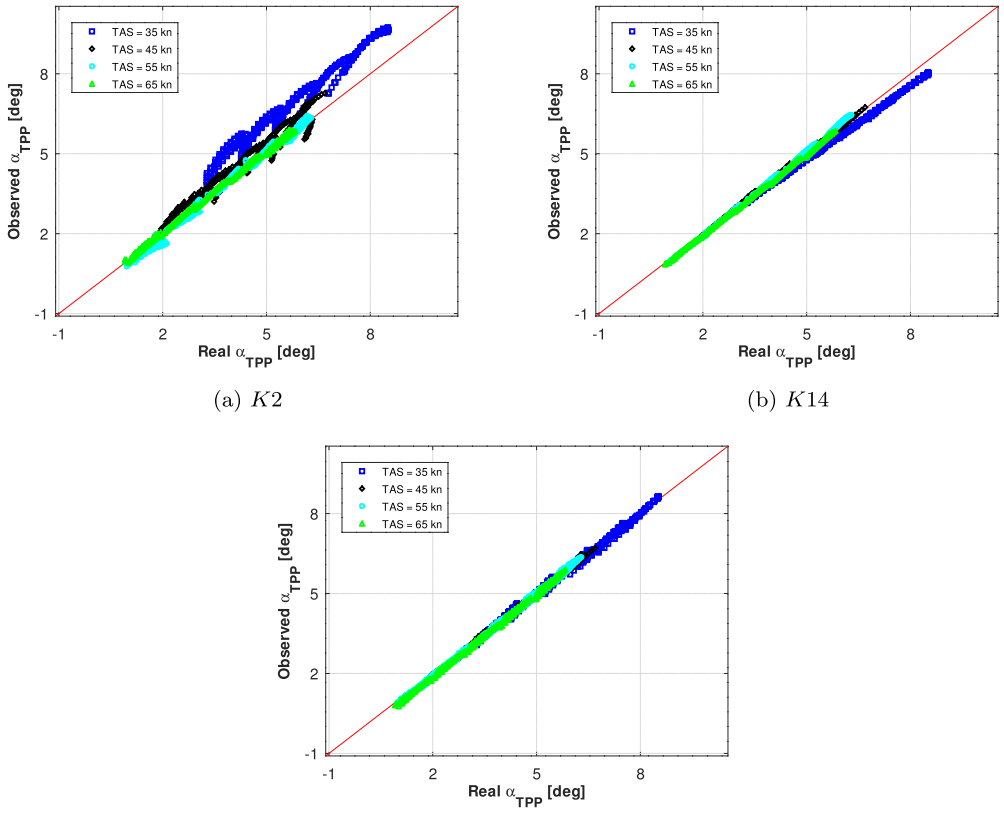

(a) $K2$ (b) $K14$

(c) $S15$

Fig. 4. Observation quality check for α_{TPP} at intermediate airspeeds.

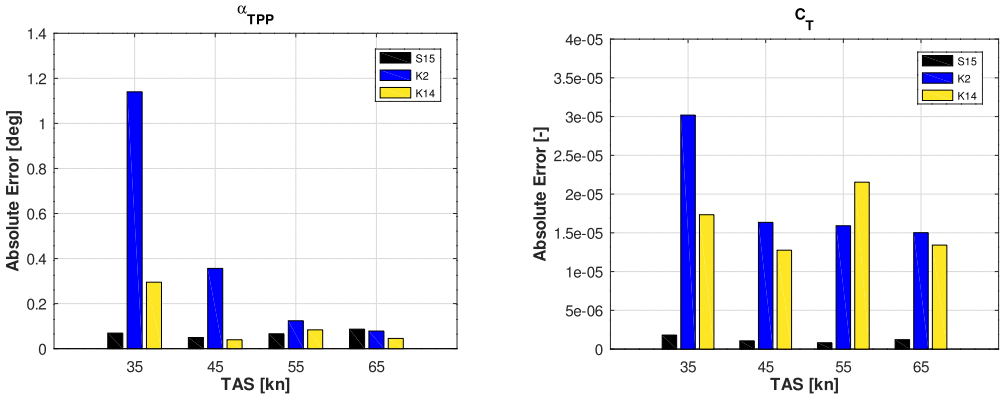

(a) Error on α_{TPP} (b) Error on C_T

Fig. 5. Average absolute error for observations at intermediate airspeeds.

- Decelerated descents
- Unsteady manoeuvres

These tests of the observer on decelerated descents and unsteady manoeuvres represent quite a variation with respect to the samples used for the identification phase, i.e. trimmed steady descent flights. Nevertheless, the magnitude of deceleration and descent profile changes remain limited. Additional analyses should look at how the observation error increases as the flown trajectory progressively departs from nominal conditions. For instance, the magnitude of the deceleration could be parametrically increased, or additional unsteady manoeuvres could be defined, involving flight conditions at increasing load factors.

5.5.1. Decelerated descents

In this first off-design scenario, the helicopter is considered following a decelerated descent trajectory. This flight condition is extremely important, since is one of the most recurrent and likely for a helicopter in real-life operation. Two possible subcases have been investigated:

- Decelerated descent with an initial airspeed V_{in} =70 kn and a final airspeed V_{fin} =50 kn
- Decelerated descent with an initial airspeed V_{in} =50 kn and a final airspeed V_{fin} =30 kn

The manoeuvre starts at an altitude $z =$ 3,000 ft and ends at the final altitude $z =$ 500 ft. The helicopter is assumed to end

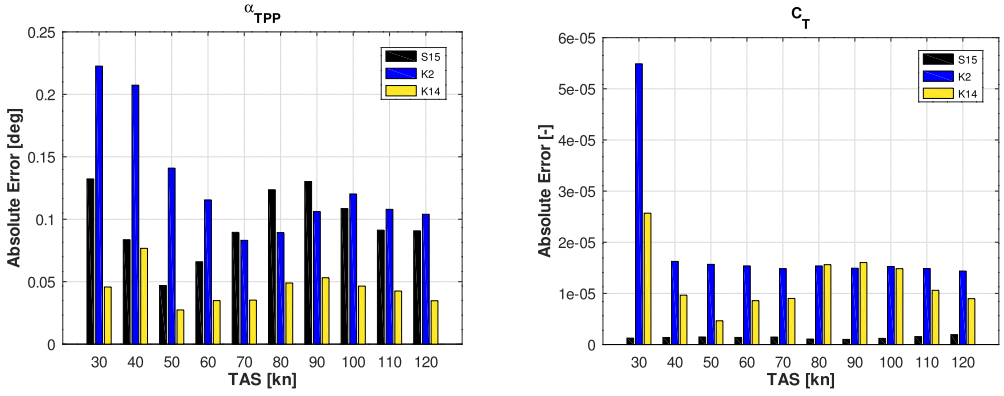

(a) Error on α_{TPP} (b) Error on C_T

Fig. 6. Average absolute error for observations at intermediate sideslip angle.

Table 5
Flight parameters considered for off-design observation phase.

$V_{in} \div V_{fin}$ [kn]	Δt_d [s]	W [kg]
50 ÷ 30	300	2,183
70 ÷ 50	350	2,381
	400	2,580
	450	2,778
		2,977
		3,175

Table 6
Conditions for model identification in a desampled scenario.

V [kn]	β_f [°]	W [kg]	z [ft]	γ_f [°]
30	-10	2,183	3,000	3
40	0	3,175	500	7
50	10			
60				
70				
80				
90				
100				
110				
120				

the descent in an amount of time Δt_d. The values of Δt_d considered are 300, 350, 400 and 450 s, yielding four different constant descent rates. Due to the time evolution imposed on the total airspeed of the helicopter and to the constraint on the vertical speed, the descent angle is not constant during the simulation. As far as it concerns the weight, values between 68.75%W_{ref} and 100%W_{ref} with a 6.25%W_{ref} increments were considered, where $W_{ref} = 3{,}175$ kg is the helicopter reference weight. A total of 48 manoeuvres were simulated and summarised in Table 5.

Results from these scenarios are presented in Figs. 7 and 8. Blue squares are decelerated descents from 50 to 30 kn, while black diamonds are decelerated descents from 70 to 50 kn. The accuracy of α_{TPP} and C_T observation is still good in all cases, for all the observer models. Still, $S15$ emerges globally as most accurate, with very low dispersion of data points around the ideal correlation line, as in Fig. 7(c), and little loss of accuracy in all the study cases, for both α_{TPP} and C_T, as in Fig. 8.

5.5.2. Unsteady manoeuvre

As an additional test, a specifically designed unsteady manoeuvre is simulated to prove the off-design performance of the observer. The unsteady manoeuvre consists of four phases:

1. steady level flight at 90 kn for 10 s;
2. uniform deceleration in level flight for 40 s, slowing down from 90 to 50 kn;
3. steady descent with 9° descent angle for 30 s;
4. transition to steady level flight at 50 kn for 20 s.

In Fig. 9 the time histories of altitude, TAS, and descent angle (γ_f) of the unsteady manoeuvre are represented.

Figs. 10 and 11 show the time histories of the α_{TPP} and C_T observations for the three models $K2$, $K14$ and $S15$. The real value of the parameter is represented by the continuous blue line, while the dotted blue line represents the observed value.

Looking at the figures, it turns out that model $K2$ is by far the least accurate in both α_{TPP} and C_T estimations. Especially, this model exhibits significant overshoots for α_{TPP} when the real value undergoes abrupt changes.

The accuracy of the other two models in estimating α_{TPP} is comparable, but model $S15$ performs better in estimating C_T.

5.6. Sensitivity to the number of samples

This last subsection examines how the quality of the observer is impacted by a decrease in the quantity of data points (i.e. a desampling) employed during the identification phase to estimate the model matrix $\boldsymbol{K}$.

As pointed out, this analysis is particularly significant, since in a real-life application of the observer, the necessary data for its synthesis could be accrued with flight test campaigns reproducing the identification manoeuvres described in Section 5.1. In this case, the considerable number of required flight tests would amount to 9,900 descents at different airspeed and sideslip angles. This would make the synthesis of the observer through experimental data an impossible task. In such case, it would be necessary to dramatically cut the number of test cases to accomplish the model identification.

For this analysis on desampling, the $K2$ model has been left out due to its performance, which is often substantially poorer than that of the other two models $K14$ and $S15$.

The same unsteady manoeuvre considered in Section 5.5.2 is chosen as the reference testing condition, since it puts the highest demands on the model adaptability.

A substantial desampling has been attempted, as reported in Table 6. This process produces a very important reduction of the amount of required input data, as reported in Table 7. Such a drastic reduction in the number of simulations and data points would allow for conspicuous savings of both costs and human effort.

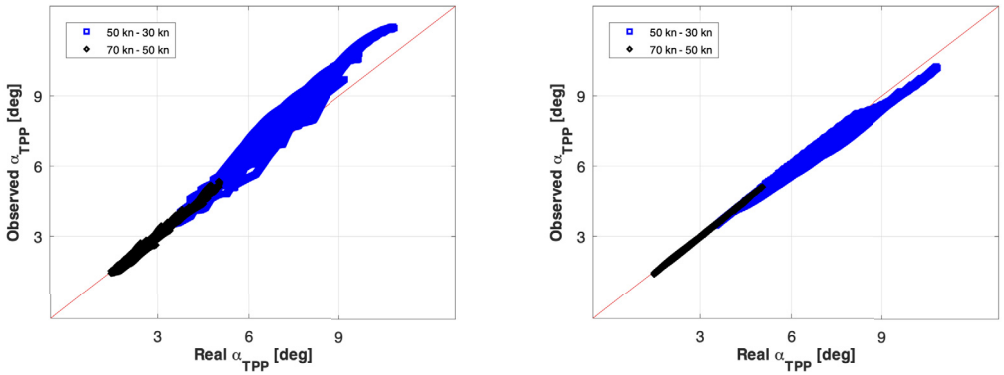

(a) $K2$ (b) $K14$

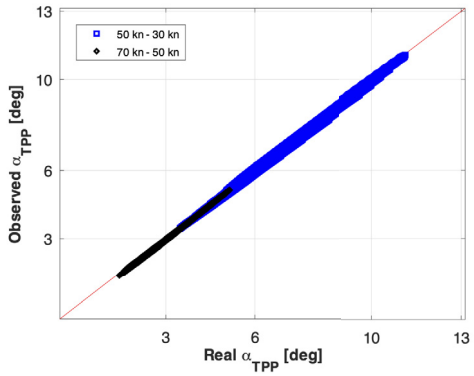

(c) $S15$

Fig. 7. Observation quality check for α_{TPP} in decelerated descents.

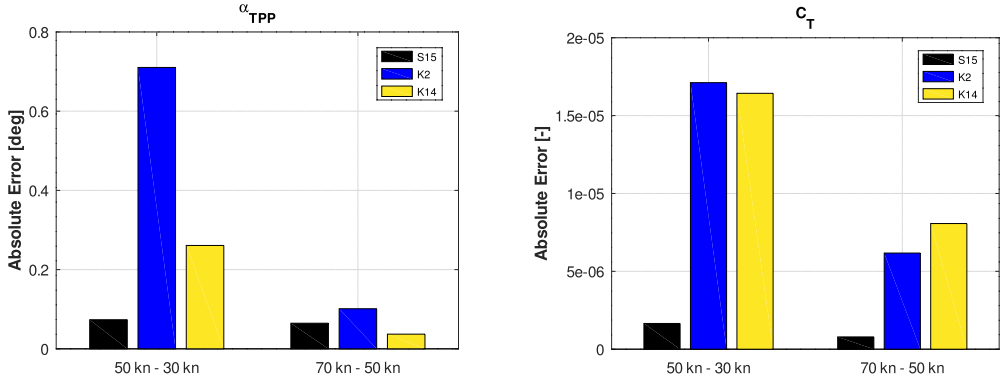

(a) Error on α_{TPP} (b) Error on C_T

Fig. 8. Average absolute error in decelerated descents.

Table 7
Comparison of the size of the original and desampled datasets.

Dataset	γ_f	W	z	β_f	Total of samples per TAS value
Standard	5	11	6	3	990
Desampled	2	2	2	3	24

The time histories in Figs. 12 and 13 show the application of the $K14$ and $S15$ models, equally desampled as in Table 7.

The graphs show that the $K14$ model observations, for both α_{TPP} in Fig. 12(a) and C_T in Fig. 13(a), are severely affected by the desampling. Specifically, the $K14$ model is no longer able to correctly observe the desired quantities in a satisfactory way, especially in the first seconds of the levelled deceleration manoeuvre at the beginning of the time history, before the descent begins. On the other hand, $S15$ model shows no particular reduction in its accuracy.

6. Discussion and conclusion

The potential of an observer for the main rotor tip-path-plane angle of attack and thrust coefficient of a helicopter has been further explored in this work, expanding previous research aiming at an increase in observation accuracy and practical applicability in the field.

After reinstating the theoretical grounds working as a base for the observer concept, its structure has been reconsidered following two directions.

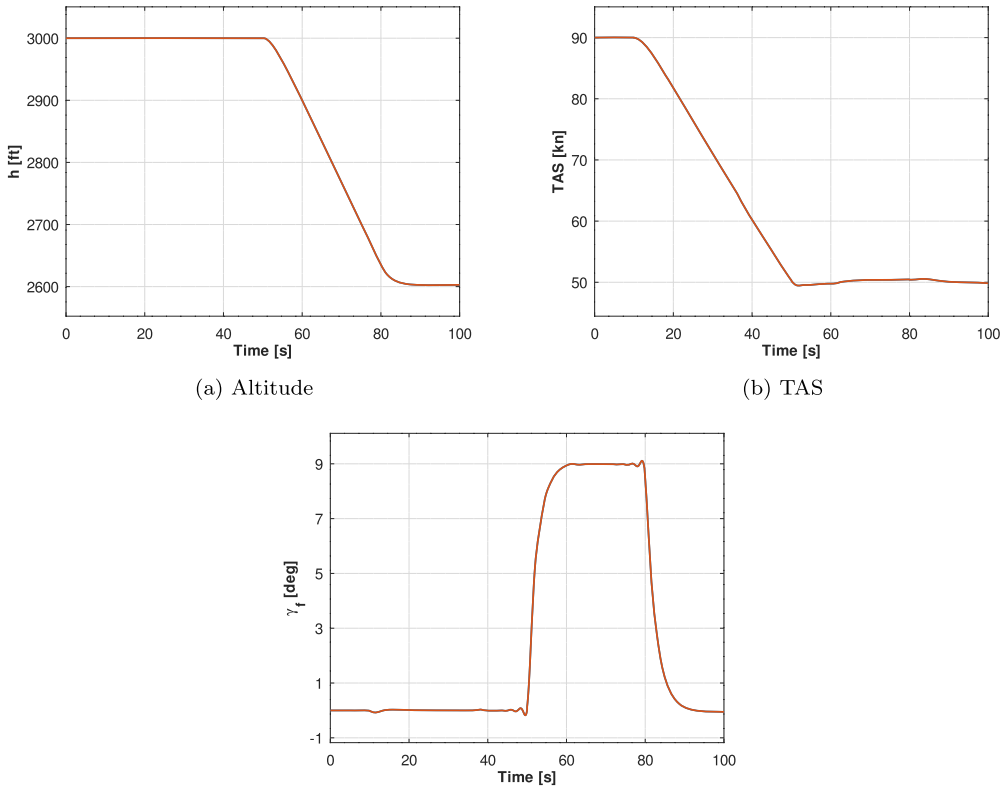

(a) Altitude (b) TAS

(c) Descent angle

Fig. 9. Time histories of the unsteady manoeuvre.

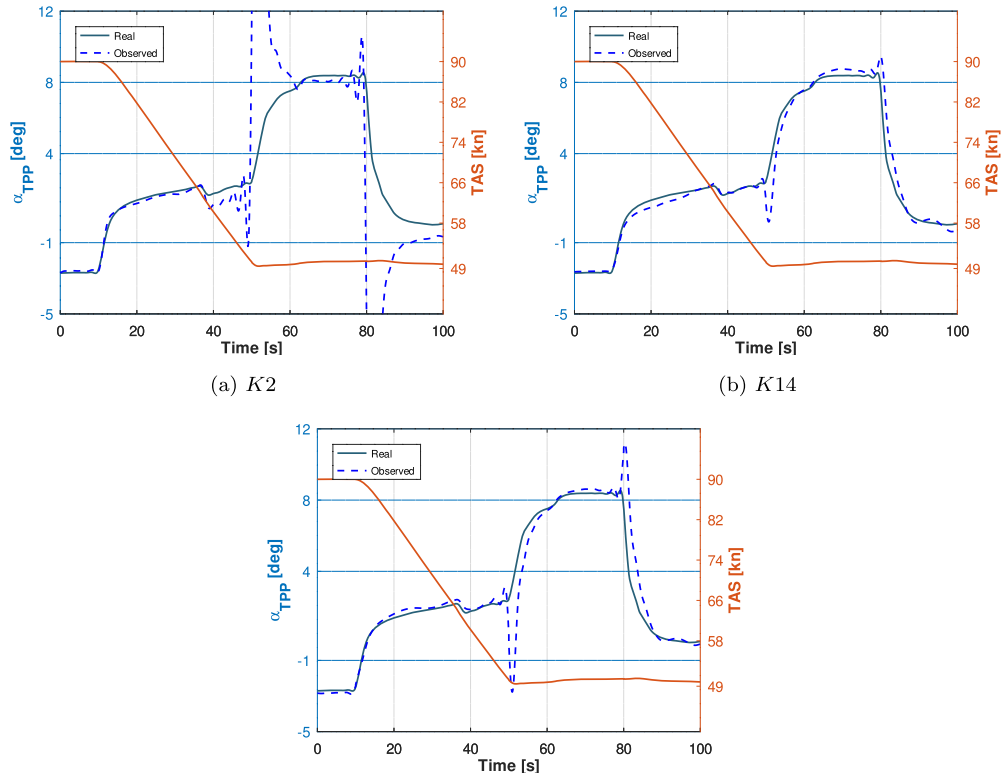

(a) $K2$ (b) $K14$

(c) $S15$

Fig. 10. Time histories of the real and observed values of α_{TPP} in the unsteady manoeuvre.

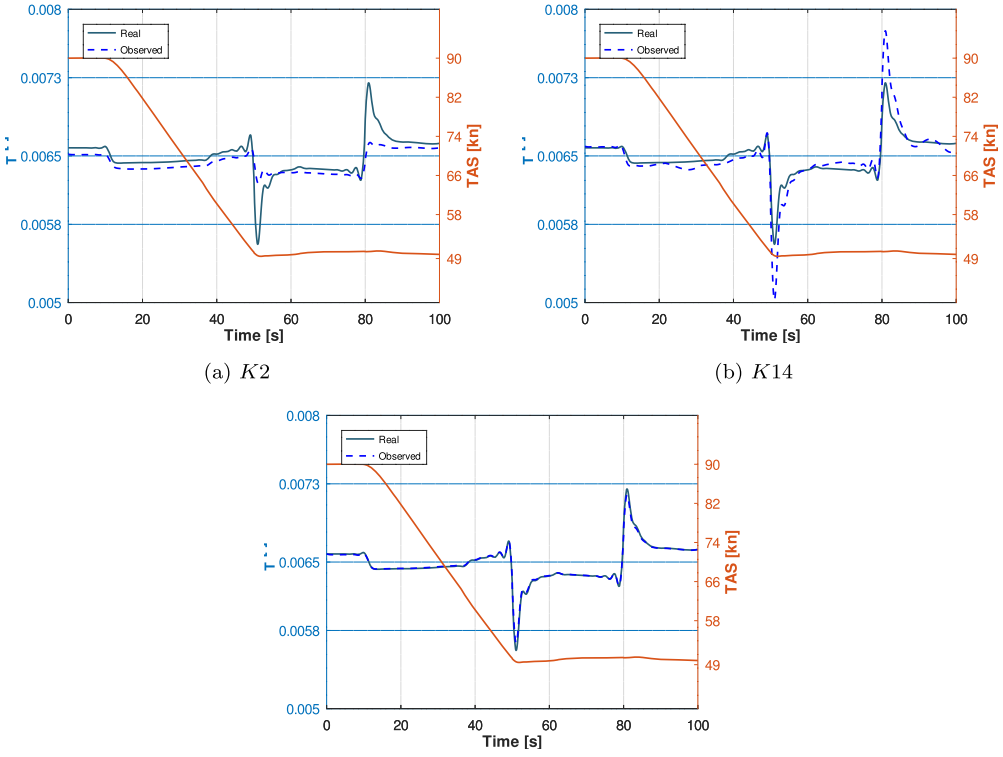

(a) $K2$ (b) $K14$

(c) $S15$

Fig. 11. Time histories of the real and observed values of C_T in the unsteady manoeuvre.

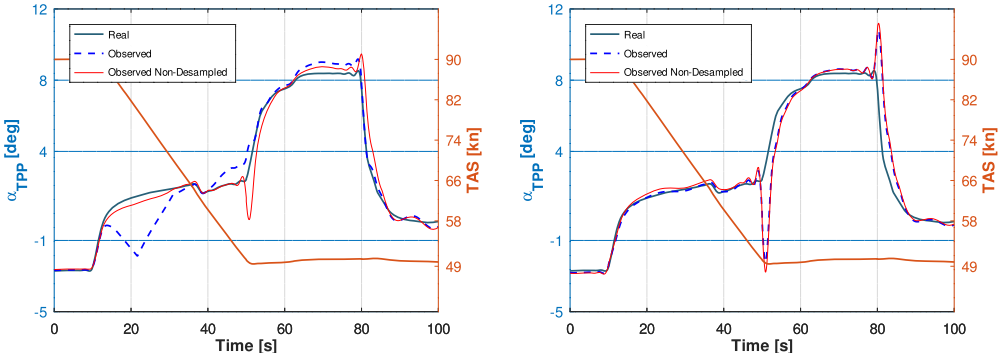

(a) $K14$ (b) $S15$

Fig. 12. Time histories of the real and observed values of α_{TPP} in the reference unsteady manoeuvre - desampled case.

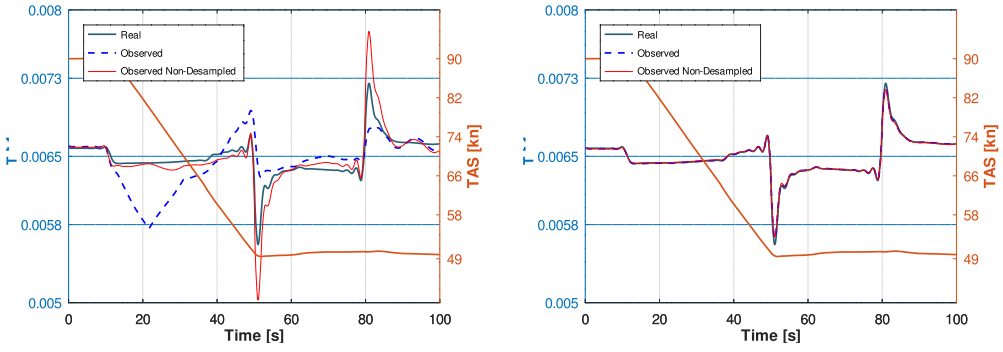

(a) $K14$ (b) $S15$

Fig. 13. Time histories of the real and observed values of C_T in the reference unsteady manoeuvre - desampled case.

First, the impact of expanding the set of measurements to include several flight mechanics parameters has been investigated.

Second, the observer structure has been emended, to include the dynamic pressure as an additional measurement, thus overcoming the high sensitivity of the model coefficients to airspeed.

The overall findings demonstrate that a linear observer model can achieve a very high level of accuracy in monitoring non-measurable properties of the main rotor if provided with a proper selection of input variables.

Results show a comparison between three different observer models. The first is the baseline model $K2$, which employs a smaller number of input measurements, whereas the other two have been shortlisted as the most promising from a broader experimentation campaign, and are namely the augmented model $K14$, and the split model $S15$. Additional research has been done to determine which is best for adoption in practical applications.

When $K2$ is compared against $K14$ and $S15$, it emerges that recurring to a sufficient number of input variables — even if they are not part of the theoretical model but suggested by practice — improves greatly the quality of the result, especially for α_{TPP} estimation. This initial finding shifts the focus on those models with the highest number of input variables, i.e. $K14$ and $S15$.

The comparison between the latter two models demonstrates how sensitive the accuracy and adaptability of the model is to the scheduling of the model coefficients with respect to airspeed or altitude.

In particular, the scheduling option with respect to airspeed, adopted for both models $K2$, $K14$ and for many intermediate models between these two, which, for brevity, have not been discussed in the paper, displays high accuracy when tested on the same data samples used for the identification process. However, these models demonstrate unsatisfactory adaptability, when faced with flight conditions that differ from those employed for identification, and particularly when non-trimmed conditions are considered.

Interestingly, model $S15$, which was constructed using a different scheduling technique depending on the observation variable (no airspeed scheduling for α_{TPP} and air density buckets for C_T estimation), turns out to be more accurate in the observation cases, especially in unsteady flight conditions, but less accurate on the identification dataset checks.

Model $S15$ has additionally demonstrated a high tolerance to substantial reductions in the number of samples used to carry out the model identification phase. This makes it possible to considerably reduce the amount of necessary input data. The robustness of the $S15$ model may provide for a significant cost reduction if real flight test data were to be employed to deliver the model identification part, drastically cutting the related costs and effort.

Considering that helicopters usually experience non-trimmed flight conditions in real-life scenarios, and given the substantial amount of data points required to synthesise the observer, it is reasonable to conclude that model $S15$ would be the most appropriate choice for the synthesis of a numerical observer of the TPP-AOA and the main rotor thrust coefficient.

Future analyses will concentrate on three aspects that emerged by examining the results:

1. Including biases in the array of measured parameters. An assessment of the observer accuracy will be done by considering the complete propagation of uncertainties in each of the measurement, especially in light of a possible real-life application.
2. Improving the behaviour of the observer during unsteady manoeuvres. This will be done by quantifying the rate of growth of the estimation error as the flight trajectory departs from the nominal steady descents. The possibility of adding selected unsteady manoeuvres among the identification samples and the effect of pitch and roll rates on flap angles will be investigated.
3. Observing more non-measurable variables from the same array of measurements. Other quantities of interest might be the fuselage aerodynamic angles, such as the fuselage angle of attack, and the sideslip angle. While the value of the fuselage angle of attack is algebraically correlated to the value of TPP-AOA, the angle of sideslip needs an extension of the observer model matrix, possibly requiring dedicated simulations to properly identify the coefficients of the model.

Declaration of competing interest

The authors declare that they have no known competing financial interests or personal relationships that could have appeared to influence the work reported in this paper.

Data availability

The data that has been used is confidential.

References

[1] L. Trainelli, M. Gennaretti, E. Zappa, M. Lovera, A.L.M. Rolando, P. Cordisco, R. Grassetti, M. Redaelli, Development and testing of innovative solutions for helicopter in-flight noise monitoring and enhanced control based on rotor state measurements, in: 42nd European Rotorcraft Forum (ERF 2016), Curran Associated, 2016, pp. 409–418.
[2] A.L.M. Rolando, F. Rossi, C. Riboldi, L. Trainelli, R. Grassetti, D. Leonello, M. Redaelli, et al., The pilot acoustic indicator: a novel cockpit instrument for the greener helicopter pilot, in: 41st European Rotorcraft Forum, Curran Associated, 2015, pp. 1228–1241.
[3] M. Gennaretti, G. Bernardini, J. Serafini, L. Trainelli, A. Rolando, A. Scandroglio, L. Riviello, E. Paolone, Acoustic prediction of helicopter unsteady manoeuvres, in: 41st European Rotorcraft Forum, 2015.
[4] L. Trainelli, M. Gennaretti, G. Bernardini, A. Rolando, C.E.D. Riboldi, M. Redaelli, L. Riviello, A. Scandroglio, Innovative helicopter in-flight noise monitoring systems enabled by rotor-state measurements, Noise Mapping 3 (1) (2016).
[5] L. Trainelli, C.E.D. Riboldi, M. Bucari, Observing the angle of attack of the tip-path plane from rotor blade measurements, in: 41st European Rotorcraft Forum, Curran Associated, 2015, pp. 1190–1201.
[6] L. Trainelli, C.E.D. Riboldi, F. Salucci, Developing an observation methodology for non-measurable rotorcraft states, in: 43rd European Rotorcraft Forum (ERF 2017), Curran Associated, 2017, pp. 370–379.
[7] C.L. Bottasso, C.E.D. Riboldi, Estimation of wind misalignment and vertical shear from blade loads, Renew. Energy 62 (2014) 293–302.
[8] C.L. Bottasso, C.E.D. Riboldi, Validation of a wind misalignment observer using field test data, Renew. Energy 74 (2015) 298–306.
[9] B.L. Stevens, F.L. Lewis, E.N. Johnson, Aircraft Control and Simulation: Dynamics, Controls Design, and Autonomous Systems, 3rd edition, Wiley-Blackwell, 2015.
[10] B. Mettler, M.B. Tischler, T. Kanade, System identification of small-size unmanned helicopter dynamics, in: 55th American Helicopter Society Forum, Montreal, Quebec, American Helicopter Society, Inc., 1999, pp. 1–12.
[11] B. Kim, Y. Chang, M. Lee, System identification and 6-dof controller design of unmanned model helicopter, JSME Int. J. 49 (2006) 1048–1057.
[12] C.E.D. Riboldi, L. Trainelli, C. Capocchiano, S. Cacciola, A model-based design framework for rotorcraft trim control laws, in: 43rd European Rotorcraft Forum (ERF 2017), Curran Associates, 2017, pp. 1–15.
[13] R.W. Prouty, Helicopter Performance, Stability, and Control, Krieger Pub Co, 1995.
[14] G.D. Padfield, Helicopter Flight Dynamics: The Theory and Application of Flying Qualities and Simulation Modelling, John Wiley & Sons, 2008.
[15] M. Fogazzi, Validation of a rotorcraft simulation tool and application to the observation of non-measurable flight parameters, Master's thesis, Politecnico di Milano, 2019.